

1
2

3

4

5 European Heliospheric FORecasting Information Asset 2.0

6 Stefaan Poedts^{1,12*}, Andrea Lani¹, Camilla Scolini^{1,2}, Christine Verbeke¹, Nicolas Wijssen¹,
7 Giovanni Lapenta¹, Brecht Laperre¹, Dimitrios Millas¹, Maria Elena Innocenti¹, Emmanuel
8 Chané¹, Tinatin Baratashvili¹, Evangelia Samara¹, Ronald Van der Linden², Luciano
9 Rodriguez², Petra Vanlommel², Rami Vainio³, Alexandr Afanasiev³, Emilia Kilpua⁴, Jens
10 Pomoell⁴, Ranadeep Sarkar⁴, Angels Aran⁵, Blai Sanahuja⁵, Josep M. Paredes⁵, Ellen Clarke⁶,
11 Alan Thomson⁶, Alexis Rouillard⁷, Rui Pinto⁷, Aurélie Marchaudon⁷, Pierre-Louis Blelly⁷,
12 Blandine Gorce⁷, Illya Plotnikov⁷, Athanasios Kouloumvakos⁷, Bernd Heber⁸, Konstantin
13 Herbst⁸, Andrey Kochanov⁹, Joachim Raeder¹⁰, Jan Depauw¹¹

14

15 ¹ KU Leuven, Leuven, Belgium

16 ² Royal Observatory of Belgium, Ukkel, Belgium

17 ³ Turun yliopisto (Finland)

18 ⁴ Helsingin yliopisto (Finland)

19 ⁵ Universitat de Barcelona (Spain)

20 ⁶ British Geological Survey (UK)

21 ⁷ Institut de Recherche en Astrophysique et Planétologie (IRAP, CNRS, Université de
22 Toulouse et CNES, France)

23 ⁸ Christian-Albrechts-Universität zu Kiel (Germany)

24 ⁹ Andrey Kochanov (company, Belgium)

25 ¹⁰ Space Consulting International LLC (company, USA)

26 ¹¹ Space Applications Services (company, Belgium)

27 ¹² Institute of Physics, University of Maria Curie-Skłodowska, Lublin, Poland

28

29

30 [*Stefaan.Poedts@kuleuven.be](mailto:Stefaan.Poedts@kuleuven.be)

31

32 Short title (running head): EUHFORIA 2.0

33

34

35 **Abstract**

36

37 **Aims**

38 This paper presents a H2020 project aimed at developing an advanced space weather
39 forecasting tool, combining the MagnetoHydroDynamic (MHD) solar wind and Coronal
40 Mass Ejection (CME) evolution modelling with Solar Energetic Particle (SEP) transport and
41 acceleration model(s). The EUHFORIA 2.0 project will address the geoeffectiveness of
42 impacts and mitigation to avoid (part of the) damage, including that of extreme events,
43 related to solar eruptions, solar wind streams, and SEPs, with particular emphasis on its
44 application to forecast Geomagnetically Induced Currents (GICs) and radiation on geospace.

45

46 **Methods**

47 We will apply innovative methods and state-of-the-art numerical techniques to extend the
48 recent heliospheric solar wind and CME propagation model EUHFORIA with two integrated
49 key facilities that are crucial for improving its predictive power and reliability, namely 1)
50 data-driven flux-rope CME models, and 2) physics-based, self-consistent SEP models for the
51 acceleration and transport of particles along and across the magnetic field lines. This
52 involves the novel coupling of advanced space weather models. In addition, after validating
53 the upgraded EUHFORIA/SEP model, it will be coupled to existing models for GICs and
54 atmospheric radiation transport models. This will result in a reliable prediction tool for
55 radiation hazards from SEP events, affecting astronauts, passengers and crew in high-flying
56 aircraft, and the impact of space weather events on power grid infrastructure,
57 telecommunication, and navigation satellites. Finally, this innovative tool will be integrated
58 into both the Virtual Space Weather Modeling Centre (VSWMC, ESA) and the space weather
59 forecasting procedures at the ESA SSCC in Ukkel (Belgium), so that it will be available to the
60 space weather community and effectively used for improved predictions and forecasts of the
61 evolution of CME magnetic structures and their impact on Earth.

62

63 **Results**

64 The results of the first six months of the EU H2020 project are presented here. These
65 concern alternative coronal models, the application of adaptive mesh refinement techniques
66 in the heliospheric part of EUHFORIA, alternative flux-rope CME models, evaluation of
67 data-assimilation based on Karman filtering for the solar wind modelling, and a feasibility
68 study of the integration of SEP models.

69

70

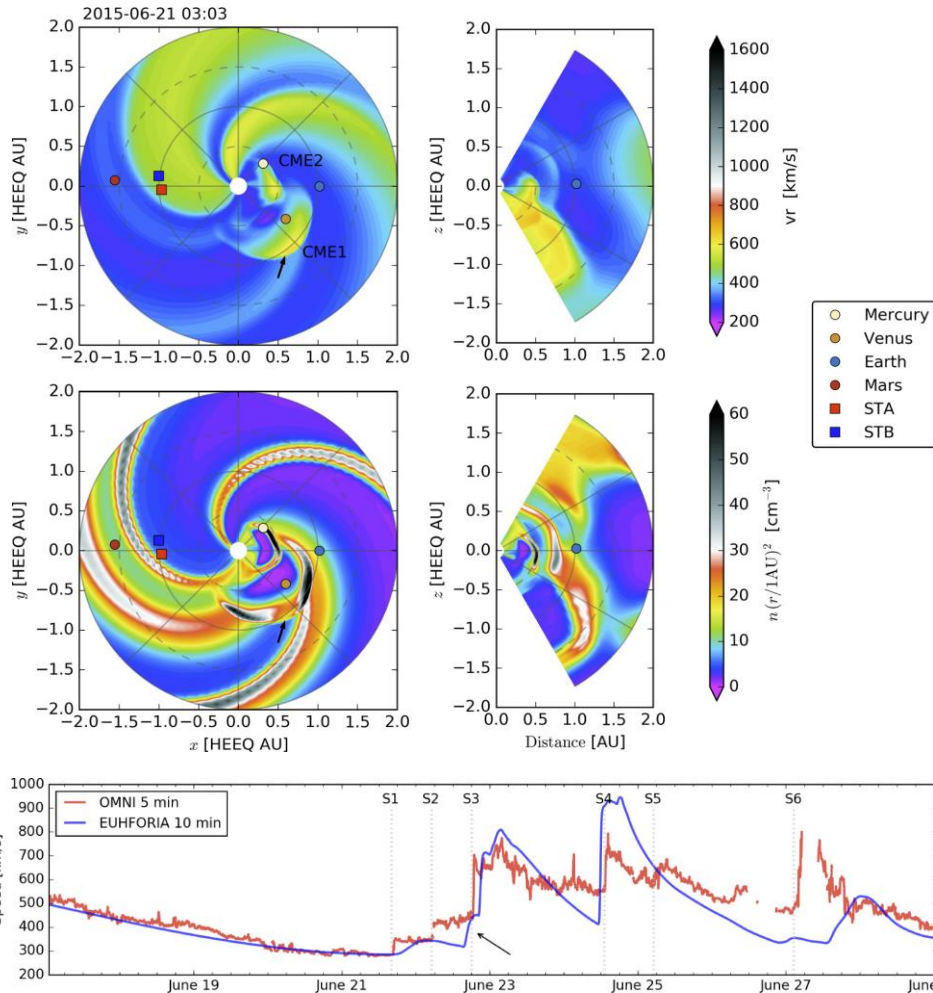
71 **1 GENERAL DESCRIPTION AND OBJECTIVE(S)**

72 **1.1 Aims and motivation**

73 The EUHFORIA 2.0 project aims at developing an advanced space weather forecasting tool.
74 The project addresses the geoeffectiveness of the impacts of CMEs, CIRs, and SEPs and
75 mitigation of (part of) the damage these cause. It also considers extreme events, but the
76 emphasis is on improving the prediction of ‘normal’ space weather and its effects, in
77 particular on its applications to forecast Geomagnetically Induced Currents (GICs) and
78 radiation on geospace. The project thus addresses many challenging aspects of space weather

79 that are interlinked in a complicated way from Sun to Earth and provides therefore also the
 80 potential for some scientific breakthroughs.

81
 82



83

Figure 1: Above: Snapshot of a EUHFORIA simulation at 03:03 UT on June 21, 2015. Below: radial velocity at L1 as measured (red) and simulated (blue) from (Pomoell & Poedts 2018)

84

85
 86
 87

88
 89 Our society is becoming increasingly dependent on technologies and infrastructures that the
 90 different space weather phenomena can damage, including power grids, satellites in orbit,
 91 and global communication and navigation infrastructures. The ultimate driver of space
 92 weather disturbances is the Sun. The most prominent forms of solar activity are Coronal
 93 Mass Ejections (CMEs), enormous eruptions of plasma (up to 10^{13} - 10^{16} g) and magnetic field
 94 into interplanetary space at velocities up to several thousand kilometres per second (Webb
 95 & Howard, 2012). When sampled in situ by a spacecraft, they are termed Interplanetary
 96 CMEs (ICMEs). The background solar wind is bimodal and consists of fast and slow streams,
 97 and their compressed interaction regions known as stream interaction regions (SIRs) or co-
 98 rotating interaction regions (CIRs) (e.g., Owens and Forsyth 2013). Associated with these
 99 bulk plasma phenomena are high-energy particle populations known as Solar Energetic

100 Particle (SEP) events (e.g., Lario and Simnett 2004), which originate through energisation
101 processes occurring at the site of solar flares and at coronal and interplanetary shocks
102 associated with CMEs, and also with SIRs/CIRs (Fisk & Lee, 1980). Desai & Giacalone (2016)
103 state that “*Solar energetic particles, or SEPs, from suprathermal (few keV) up to relativistic*
104 *(~few GeV) energies are accelerated near the Sun in at least two ways: (1) by magnetic*
105 *reconnection-driven processes during solar flares resulting in impulsive SEPs, and (2) at*
106 *fast coronal-mass-ejection-driven shock waves that produce large gradual SEP events”.*

107
108 Direct interactions of CMEs and solar wind streams with the Earth’s magnetosphere and
109 SEPs represent two very different chains, both however crucial for space weather. While
110 solar wind, CMEs, and SIRs/CIRs arrive at Earth orbit typically in one to five days, high-
111 energy SEPs arrive only in tens of minutes. In contrast to the bulk plasma propagation, SEPs
112 with energies of keV to GeV follow trajectories constrained by the Interplanetary Magnetic
113 Field (IMF) orientation. CMEs and SIRs cause disturbances in the geomagnetic field,
114 radiation environment surrounding the Earth (so-called Van Allen Belts) and various
115 current systems in the magnetosphere and ionosphere with effects reaching to the ground.

116
117 CMEs are the key drivers of strong and extreme magnetic storms. They are most important
118 at solar maximum, but can cause (extreme) storms at any phase of the solar cycle, including
119 solar minimum (e.g., storm in February 1986; Riley et al., 2012) and also during weaker solar
120 cycles (e.g., Kilpua et al., 2015; Liu et al., 2018). CIRs/SIRs, in turn, drive mainly weak to
121 moderate storms, but they effectively enhance electrons to relativistic energies in the
122 radiation belts. SEPs can penetrate the magnetosphere posing a significant threat to
123 satellites. The most energetic SEPs can penetrate even down to the upper atmosphere, where
124 they can have a significant effect on chemistry and result in an atmospheric cascade called a
125 Ground Level Enhancement (GLE). The mutual interaction of CMEs can substantially
126 increase both their potential to accelerate particles, and their geoeffectiveness (e.g., Farrugia
127 et al. 2006). In a “perfect storm” scenario (Liu et al., 2014), the first CME “clears out” the
128 ambient solar wind plasma, such that the subsequent CME will experience a minimal drag
129 and will reach Earth with high speed resulting in major space weather effects throughout the
130 terrestrial system.

131
132 Current space weather modelling tools, however, lack several crucial aspects which clearly
133 limits their forecasting capability, namely related to 1) interfacing different models from the
134 Sun to the magnetosphere and ground effects models, 2) predicting in advance the internal
135 magnetic field of Earth-impacting CMEs (this is also a vital aspect to understand and forecast
136 CME-CME interactions), and 3) having capability to predict SEP events.

137
138 The information on the solar wind conditions impacting the Earth is currently basically only
139 available at the Lagrangian point L1 from where it takes only about 30 minutes to 1 hour to
140 reach our planet, i.e., clearly less than the 1-2 days required by most space weather end users.
141 Most critically, there are no measurements or practical tools to estimate the magnetic field
142 in CMEs before they arrive at the Earth’s magnetosphere. Even a fast and strong CME
143 impacting Earth may pass with only minor effects if its magnetic field is directed mainly
144 northward. SEPs and related effects, in turn, are primarily determined by the speed, shape
145 and extent of a CME when it is launched from the Sun, as well as by the properties of the
146 ambient corona the CME surges into. Considering the effects from direct interactions, there

147 should be time to predict and mitigate their geoeffectiveness well in advance as we observe
148 the CME eruption 1-4 days before their arrival at Earth orbit. Although similar lead times
149 cannot be expected for SEPs, which propagate in some tens of minutes from the Sun to the
150 Earth in magnetically well-connected events, accurate modelling can crucially increase our
151 capability to predict the duration and severity of the solar radiation storms that have or are
152 about to commence after western flares and CMEs. For poorly connected eastern events,
153 however, physics-based modelling can significantly improve even the lead time, in
154 particular, if observations from L5 are available, which would allow one to assimilate
155 observations from a better-connected location.
156

157 **1.2 Objectives**

158
159 EUHFORIA has already been integrated into the ESA Virtual Space Weather Modelling
160 Centre (VSWMC) (Poedts 2018) and has been coupled to several other models within this
161 framework (see the example visualized in Figure 2). The VSWMC models are available to the
162 space weather user community via the [SWE portal \(http://swe.ssa.esa.int/\)](http://swe.ssa.esa.int/), the main user
163 interface of the ESA SWE network (Poedts et al. 2019).
164

165 In the EUHFORIA 2.0 project, we will make several critical improvements to EUHFORIA.
166 Our main focus here is on the most urgent physical challenges and damaging impacts that
167 can be mitigated. Thus, the **specific objectives** are:

168 **Objective 1.** To provide accurate predictions of plasma and magnetic field in the Near-
169 Earth solar wind by improving our heliospheric wind and CME evolution
170 model EUHFORIA by *implementing data-assimilation techniques (using both*
171 *available and potential L5 and Solar Orbiter data) as well as determine the*
172 *internal magnetic structure of CMEs using advanced flux-rope models*
173 *constrained by data-driven and machine learning techniques.*

174 **Objective 2.** To *develop a global coronal MagnetoHydroDynamics (MHD) model for*
175 *EUHFORIA, capable of quantifying the source regions of CMEs and the global*
176 *coronal magnetic field.*

177 **Objective 3.** To *integrate current state-of-the-art SEP transport models in EUHFORIA*
178 *for simulation of SEP emission from coronal shocks and to develop*
179 *methodology and tools for predicting the SEP emission from CMEs.*

180 **Objective 4.** To *develop an operational prediction tool for GICs in power grids.*

181 **Objective 5.** To *develop more reliable operational prediction tools for harsh radiation in*
182 *geospace.*

183 **Objective 6.** To *exploit EUHFORIA by creating completely novel space weather*
184 *forecasting service facilities tailored carefully to the needs of selected target*
185 *groups.*

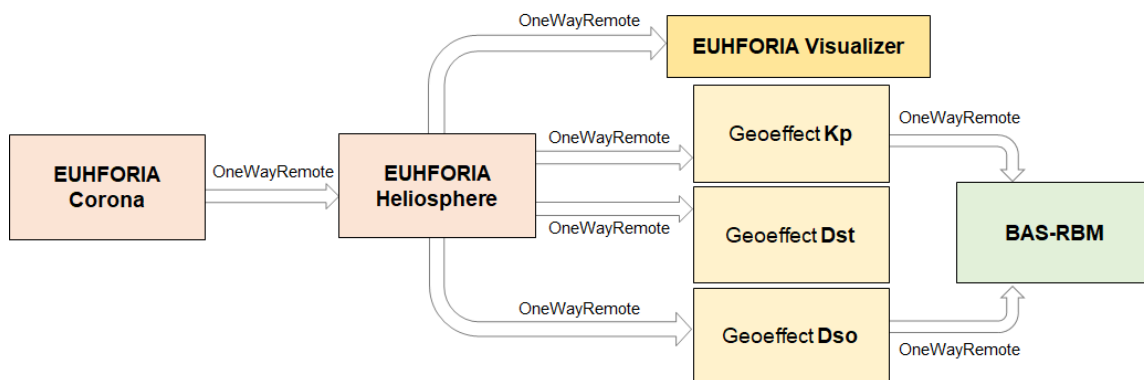


Figure 2: One of the Sun-to-Earth modelling chains implemented in the VSWMC that became operational in 2019 (see Poedts et al. (2019)). In this chain EUHFORIA is coupled to models to determine the Kp and Dst indices and the plasma sphere stand-off distance, based on the synthetic wind data at L1 from EUHFORIA. The Kp index and the plasma sphere stand-off distance (Dso) are then used to drive the British Antarctic Survey Radiation Belt Model.

186
187
188
189
190
191
192

193 Referring to the modelling chain in Figure 2, we will replace the coronal model in
194 EUHFORIA with a more advanced one, improve the heliospheric part of EUHFORIA (using
195 data assimilation techniques), and couple our SEP transport and acceleration models to
196 EUHFORIA so that we put the SEP source much closer to the Sun and capture the high-
197 energy events too. The concept has been proven already (Wijzen et al. 2019a,b, see below).
198 Moreover, in addition to the geo-indices models mentioned in Figure 2, we will couple a
199 magnetospheric model (OpenGGCM) and GIC and radiation models to EUHFORIA 2.0. *This*
200 *will enable us to replace the nowcasts given by these models to forecasts with up to 5 days'*
201 *notice.*

202 To maximise the impact, our dissemination and exploitation plan is tailored carefully to the
203 needs of the target groups. The EUHFORIA 2.0 forecast tool will provide reliable
204 quantitative predictions of the space environment parameters at L1 and other satellite
205 positions in the solar system, and forecast GICs in elements of the interconnected European
206 power grid and radiation in the ISS, satellites and public airplanes.

207 1.3 Key science questions

208 The **Key Science questions** of the EUHFORIA 2.0 are also inspired by COSPAR roadmap
209 recommendations (Schrijver et al. 2015):

- 210 1. *What is the global coronal field that drives the solar-wind plasma and magnetic field*
211 *from Sun to Earth and what coronal parameters affect the solar wind at 1 AU the most?*
- 212 2. *How and to what extent do the initial eruption features and the interaction with the*
213 *solar wind affect (erode, deform) the properties and geoeffectivity of CME-driven IP*
214 *shocks and ICMEs?*
- 215 3. *How are SEPs produced and transported to 1 AU over the course of CMEs?*
- 216 4. *To what extent does the ambient solar wind play a role in determining whether we*
217 *observe large SEP events when a big and fast CME event occurs?*
- 218 5. *What are the factors which control the generation of geomagnetically-induced currents*
219 *(GICs) and of harsh radiation in geospace (involving the coupling of solar wind*

220 *disturbances to internal magnetospheric processes in the magnetosphere and the*
221 *ionosphere below)?*

222

223

224 **2 CONCEPT AND METHODOLOGY**

225 **2.1 Project concept**

226 Interplanetary CMEs (ICMEs) are the main drivers of space weather. Therefore, the
227 modelling of CME onset, SEP emission, and their interplanetary propagation up to the
228 impact on the Earth's magnetosphere (affecting the ionosphere, thermosphere, radiation
229 belts, etc.) is pivotal for reliable space weather forecasts. Regional warning centres, e.g. in
230 Brussels (at the Royal Observatory of Belgium), provide daily forecasts using several semi-
231 empirical and simulation models that have been developed for this purpose. *There are,*
232 *however, two major problems related to our current forecasting capabilities.* First of all,
233 many of the currently available space weather models are oversimplified, leaving out some
234 key physics, because these are complicated (multi-scale/multi-physics) and/or CPU
235 demanding. The second problem lies in interfacing the different models related to the
236 different domains involved (e.g., the solar corona, the heliospheric solar wind, the CME
237 onset and propagation, SEP events, the terrestrial magnetosphere and ionosphere, etc.) in a
238 consistent coupling framework. Therefore, a SEP prediction model needs to be coupled to
239 the CME propagation and impact model and a comparison between observations and
240 simulation outputs must be carried out to validate any new or upgraded model.

241 Current CME propagation models, including ENLIL (Odstreil, 2003) and SUSANOO (Shiota
242 and Kataoka, 2016), all have limitations: 1) they use a *very simplified background solar*
243 *wind model*, 2) they use *over-simplified CME models* that take at most marginally into
244 account the structure of the magnetic field within the CME itself; 3) they describe the CME
245 *early propagation only in a simplistic way or not at all* (when introduced only at 0.1 AU
246 like e.g., cone CME models); 4) they *do not provide any information about the SEP emission*
247 *and transport properties* generated by solar flares and the CME leading shock fronts; and
248 5) they are *not coupled with magnetospheric/ionospheric and effects models*. Recently, first
249 attempts were made to include the internal magnetic structure of the CMEs in ENLIL, in the
250 Space Weather Modelling Framework (Tóth et al., 2005), in SUSANOO (Shiota & Kataoka,
251 2016), and in EUHFORIA (Verbeke et al. 2019; Scolini et al. 2019), but none of them are yet
252 used for operational space weather forecasting

253 The EUHFORIA project offers an opportunity to build and validate a new advanced space
254 weather forecasting tool, covering both geomagnetic storms from direct interactions of
255 CMEs and other large-scale solar wind structures with the Earth's magnetic environment,
256 and the SEPs generated radiation storms. This builds on the state-of-the-art model
257 EUHFORIA, a 3D MHD solar and heliospheric model that simulates the solar wind and the
258 evolution of a superimposed CME structure from 0.1 AU to 2 AU (i.e. including the orbits of
259 both Earth and Mars) (see Figure 1; Pomoell and Poedts, 2018). Wijzen et al. (2019a,b) have
260 already combined EUHFORIA output with a novel SEP transport model solving the focused
261 transport equation with Monte Carlo techniques. At the same time, advanced numerical
262 simulation models have been developed for the acceleration and transport of particles in the

263 corona enabling to get a deeper understanding of the complexity of the interaction between
264 coronal shocks and solar magnetic fields (Afanasiev & Vainio, 2013; Afanasiev et al. 2014,
265 2015, 2018a, 2018b; Vainio et al. 2014).

266
267 In EUHFORIA, the CMEs are modelled with a magnetic flux-rope, thus taking into account
268 the crucial internal magnetic structure. This enables more reliable CME evolution
269 simulations, taking into account the effects of erosion and deflection (occurring through
270 magnetic reconnection of the internal magnetic field with the magnetic field of the ambient
271 solar wind) and deformation (due to the interaction with the ambient solar wind), and
272 predictions of the geoeffectiveness of an event (which depends largely on the sign and
273 magnitude of the Bz-component, i.e. perpendicular to the equatorial plane). It has been
274 shown that the use of a spheromak CME model significantly improves the predictions
275 (Verbeke et al. 2019; Scolini et al. 2019, 2020).

276
277 As mentioned above, all the current operational heliospheric wind and CME propagation
278 models completely ignore SEP acceleration and transport. Yet, solar energetic particle events
279 can affect communications and airline safety, and affect satellites by radiation damage to
280 electronics. Protons of more than 30 MeV could kill astronauts since these can penetrate
281 spacesuits and spacecraft walls. Hard particle energy spectra can contain large fluxes of
282 hundreds of MeV - GeV type super-energetic particles, which can reach Low Earth Orbit
283 (LEO) satellites and even penetrate into the safest areas of spacecraft. *The major innovation*
284 *of the current project will thus be the integration of state-of-the-art SEP transport and*
285 *emission models into a physics-based and self-consistent model.* This will enable to
286 understand, quantify and even forecast the origin and evolution of SEP events.
287

288 **2.2 Methodology**

289 The methodology of the proposed project is directly linked to the six specific objectives
290 mentioned in Section 1.2, namely as follows.

291 **Objective 1:** *Implementing advanced flux-rope models for the internal structure of CMEs.*

292 We will improve the current wind model in EUHFORIA using data-assimilation techniques
293 exploiting currently available satellite data and exploring the usefulness of L5 data. We will
294 also apply Machine Learning techniques to quantify the sensibility of the predictions on the
295 CME input parameters in order to optimize the ensemble modelling for the forecasts. We
296 will also explore Lagrangian methods to increase the cost-effectiveness, starting from the
297 SLURM code developed at KU Leuven (Bacchini et al. 2017), and coupling it to EUHFORIA
298 to demonstrate the ability to run a rapid simulation of CMEs.

299 A CME model should be capable of providing a reasonable 3D geometry fit, include typical
300 deformations (expansion, deflection, rotation, flattening ('pancaking'), skew (due to solar
301 rotation)), and have a 3D internal magnetic field configuration with a low, nearly constant
302 twist. We will implement the Fri3D model (Isavnin 2016) as well as other flux-rope models.

303 **Objective 2:** *Developing an improved coronal model for EUHFORIA.*

304 This objective will be tackled by developing novel *models of the solar coronal magnetic field*
305 *and plasma environment and tools to determine realistic initial CME and shock*
306 *parameters* from the low corona up to 0.1 AU. We will develop an advanced MHD-based
307 model of the solar corona by extending our current coronal model (Pomoell & Vainio 2012).
308 The new model will include a detailed description of coronal thermodynamics, including
309 anisotropic heat conduction, separate ion and electron temperatures and radiative losses.
310 The coronal heat input is provided by an Alfvén wave turbulence model that has shown to
311 reproduce well the coronal large-scale extreme ultraviolet emission (van der Holst et al.,
312 2014).

313 In addition, a 3D coronal shock wave propagation module will be developed to provide quick
314 modelling of shock wave properties in the corona and establish how these shocks connect to
315 specific points of interest in the inner heliosphere. This module will provide the critical shock
316 parameters modelled in 3D which will be used as inputs for the SEP emission modelling.

317 We will also develop tools for obtaining realistic and practical information of initial CME and
318 shock parameters to constrain the new flux rope models (see Objective 1) and for the SEP
319 forecasting models (see Objective 5). We explore additionally a fully data-driven modelling
320 approach of erupting coronal magnetic fields provided by the supporting UH ERC project
321 SolMAG (PI: Emilia Kilpua) to obtain CME magnetic structure self-consistently and time-
322 dependently without the intervention of the modeller (Pomoell et al. 2019, Price et al. 2019).

323
324 **Objective 3:** *Integrating current state-of-the-art SEP transport models* in EUHFORIA.

325 The University of Turku (UTU) team has developed state-of-the-art numerical simulations
326 for particle acceleration at shocks, including the *Coronal Shock Acceleration* (CSA)
327 simulation model (Vainio & Laitinen 2007), which can accommodate global heliospheric
328 field configurations. The more recent model *SOLar Particle Acceleration in Coronal Shocks*
329 (SOLPACS), uses a physically accurate description of microphysics but is presently limited
330 to local simulation volumes around the shock (Afanasiev et al. 2015). For the downstream
331 side of the shock, the UTU model suite uses a test-particle Monte Carlo simulation called
332 *DownStream Propagation Model* (DSPM), solving the Parker equation in a prescribed bulk-
333 plasma flow field with a prescribed spatial diffusion tensor.

334

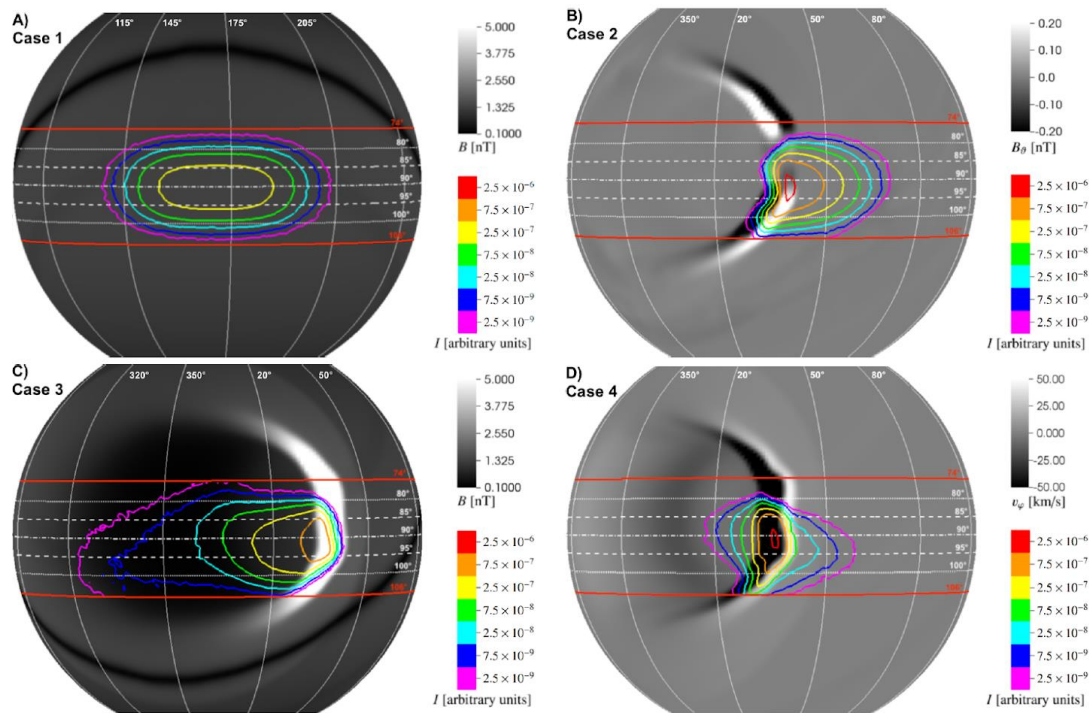


Figure 3: Contour plots of the particle intensity at $r = 1.5$ AU, drawn on top of different MHD solar wind variables, 15.5 hours after particle injection and for the simulations with cross-field diffusion. The red parallels indicate the borders of the sampling region. Four cases with different injection regions are shown. Upper left: intensities of case 1 drawn on top of the magnetic field magnitude. Upper right panel: intensities of case 2 drawn on top of the magnetic field colatitude component. Lower left panel: intensities of case 3 drawn on top of the magnetic field magnitude. Lower right panel: intensities of case 4 drawn on top of the longitudinal velocity component. (Wijsen et al. 2019b).

335
336
337
338
339
340
341
342
343

344

345 The UB team in collaboration with KU Leuven team have developed a *Shock-and-Particle*
346 (SaP) model (Pomoell et al. 2015), which is solving a focused transport equation in a Parker-
347 spiral magnetic field and constant solar wind flow. Unlike CSA/SOLPACS, SaP is not self-
348 consistent in terms of energy exchange with the scattering waves, but its advantage is that
349 the method is computationally efficient, which makes it an attractive alternative for
350 operational modelling.

351 Moreover, the KU Leuven, University of Barcelona (UB) and University of Helsinki (UH)
352 teams developed the *Particle radiation asset directed at interplanetary space exploration*
353 model (PARADISE, Wijsen (2020), see Figure 3), a Monte Carlo 3-D particle focused
354 transport model coupled with the EUHFORIA solar wind model to describe impulsive SEP
355 events in non-nominal solar wind conditions in the interplanetary domain (Wijsen et al.
356 2019a,b). Test-particle approaches are also the way to make the Monte Carlo modelling
357 compatible with operational requirements. From this variety of models, we will select the
358 best compromise between accuracy and efficiency.

359 **Objective 4:** *Developing an operational prediction tool for GICs in the EU power grid.*

360 To provide a realistic description of the ionospheric medium and to determine ionospheric
361 horizontal electrical currents, the CNRS group will use the electrodynamics model IMM
362 (Hurtaud et al. 2007), which will be coupled to the first-principles ionosphere model IPIM
363 at both high- and mid-latitudes (Blelly et al. 1996; 2005; Marchaudon and Blelly 2015). All
364 these models have been developed in the IRAP/CNRS group and have been successfully
365 coupled in the past (Blelly 2003). Fed with sufficiently accurate energy inputs, e.g. from the
366 solar wind, the coupled models give an excellent description of ionospheric dynamics at
367 speeds suitable for operational space weather forecasting and will provide accurate
368 ionospheric conductivities and currents.

369 We will also develop and couple a Biot-Savart model to these different models to provide
370 forecasts of geomagnetic variations at any point on the ground. Using this forecast model,
371 the BGS team *will simulate the flow of GICs, induced by rapid, high-amplitude magnetic*
372 *field changes, in national models that are part of the connected European and separate UK*
373 *electrical transmission systems and determine the impact on electrical substations within*
374 *these networks, including impacts within individual transformers at key locations.* We will
375 build on previous work (e.g. Thomson et al. 2005; Kelly et al. 2017; EU FP7 'EURISGIC')
376 through updated Earth conductivity models for Europe and the UK and updated electrical
377 network details that allow us to probe transformer level impacts at key substation sites
378 accurately.

379 To provide context and comparison the BGS group will compare the results of the coupled
380 EUHFORIA/CNRS model, in terms of prediction accuracy of dB/dt and predicted GIC, with
381 the dB output of an existing and tested geospace model, OpenGGCM (Raeder et al. 2017),
382 and, independently, a statistical model of 30-minute predicted peak dB/dt (Wintoft et al.
383 2015). These dB and dB/dt predictions will be coupled to a detailed UK power grid network
384 model, as a representative model for a complex national system within Europe.

385 **Objective 5:** *Developing more reliable prediction tools for harsh radiation in geospace.*

386 In order to provide a realistic description of the radiation dose in silicon and
387 tissue-equivalent material aboard the ISS and at aircraft altitudes, a concept that has
388 successfully applied to neutron monitor (NM) measurements (Bieber et al. 2004, Heber et
389 al. 2015) and dose rate computations (Mishev et al. 2015) will be adapted. The approach used
390 to interpret the NM data is based on so-called yield functions (Caballero-Lopez 2016) which
391 are computed by tracking particles through the atmosphere and determine the NM response
392 to the radiation environment caused by these particles. Different programs based on the
393 GEANT4 (Agostinelli et al. 2003) or CORSIKA library (Heck et al. 1998) have been utilised
394 computing the yield function (see Caballero-Lopez 2016). However, the yield function in the
395 rigidity range between 1 to 16 GV can be determined experimentally by latitudinal surveys
396 (Caballero-Lopez and Moraal 2012). We will follow a mixed approach. In order to determine
397 the yield function for the radiation dose in silicon, we will analyse DOSTEL measurements
398 aboard the ISS (see Labrenz et al. 2015) and aboard an aircraft (Möller et al. 2012) using
399 galactic cosmic ray spectra inferred from O'Neill (2010). In order to determine the yield
400 function in tissue-equivalent material we will set up a GEANT4 model of the DOSTEL within
401 the radiation environment that reproduces the yield in the range from 1 to 16 GV. Using our
402 (coronal+interplanetary) SEP transport model together with the detailed computation of
403 motion of charged particles in the variable Earth's magnetic field (Desorgher et al. 2006),

404 we will compute the radiation dose in silicon and in tissue during a SEP event within the ISS
405 and on typical polar routes.

406 **Objective 6:** *Creating completely novel space weather forecasting service facilities.*

407 To maximise the impact of the project, we want to *distribute the science, software and*
408 *services developed within the project to target groups* that have an interest or are impacted
409 by space weather in general. Therefore, we will disseminate a message tailored to the needs
410 of a stakeholder or client making use of the appropriate tactics and tools. We want to raise
411 awareness, reach involvement and come to a possible future collaboration.

412 Presently, various CME catalogues exist, but most of them focus only on one type of
413 observation/instrumentation, typically based on white-light coronagraph imaging. These
414 catalogues also typically provide rather basic CME parameters that are subject to projection
415 effects. A significant step in the direction of presenting combined and community-wide
416 catalogues was established in the FP7-funded HELCATS project ([https://www.helcats-
417 fp7.eu](https://www.helcats-fp7.eu)). We will use realistic information of CME coronal parameters (Objective 2) to
418 constrain flux ropes in EUHFORIA, provided by different advanced reconstruction
419 techniques and data-driven modelling that apply a wide variety of state-of-the-art remote-
420 sensing observations and also upcoming data. The results will be compared to the real data,
421 in terms of metrics for continuous and binary variables. Initial preliminary comparisons
422 have been done by Scolini et al. (2019).

423 For shocks, we will apply EUV and radio triangulation to reconstruct the shock geometry.
424 The radio triangulation techniques use direction-finding observations of the SWAVES
425 instruments on-board WIND and STEREO spacecraft. As WIND is a spinning spacecraft and
426 STEREO is a 3-axis stabilised spacecraft, different direction-finding methods will be used
427 for these spacecraft (Magdalenic et al., 2014). The results of radio triangulation will be
428 combined with white-light based reconstruction techniques in order to provide the 3D
429 picture of the CME and the radio-emitting part of the CME-driven shock wave. We will make
430 use of radio-tracking of CMEs using Type II bursts. Using the Vršnak et al. (2004) density
431 model, we will compile the distance maps of the CME-driven shock waves.

432 433 434 **3 IMPLEMENTATION AND FIRST RESULTS**

435 **3.1 Some first results of the project**

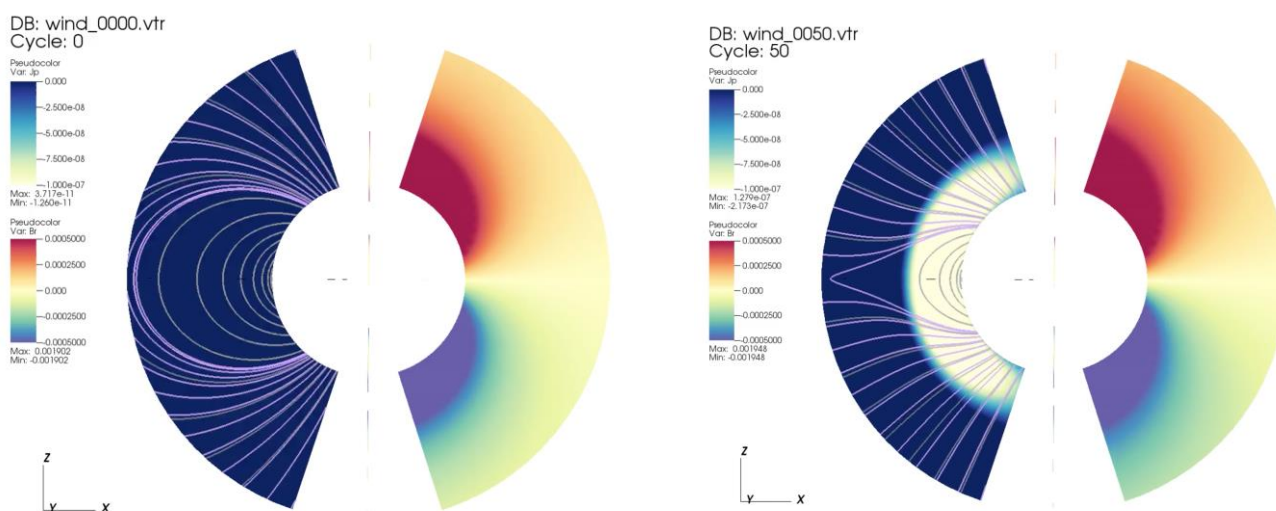
436 The EUHFORIA outreach website is online: <https://euhforia.com/> and contains information
437 on the EUHFORIA 2.0 project and on the EUHFORIA model itself, and links to the Blog and
438 the Wiki. It also contains a link to the EUHFORIA Online app
439 (<https://www.euhforiaonline.com/>). It provides a Graphical User Interface (GUI) to set all
440 the input parameters to run EUHFORIA Corona and EUHFORIA Heliosphere and provides
441 the standard output pictures and movies automatically.
442

443 Below we briefly present some of the first scientific results obtained. Papers with more
444 detailed descriptions and discussions of these results, have been submitted or are in
445 preparation.
446

447 3.1.1 Global non-potential model of the coronal magnetic field

448 The development of a global model of the coronal magnetic field as an alternative to the
449 current PFSS + Schatten current sheet model in EUHFORIA, has started. The new model is
450 based on the magneto-frictional method (MFM) for time-dependent data-driven modelling
451 of active region evolution that has been developed by Pomoell, Lumme and Kilpua (2019).
452 For the global coronal magnetic field, the MFM code has been extended to support spherical
453 geometry. Preliminary tests with the new code have been performed. Relaxation of an initial
454 dipolar magnetic field to include the effect of stretching of field lines due to the solar wind
455 has been successfully performed. The resulting magnetic field structure resembles closely
456 those obtained from MHD-based coronal models, incl. an open streamer belt (Figure 4).

457
458 As an example application of more advanced boundary conditions, a second test involving
459 the energization of the coronal magnetic field via build-up of currents in the coronal
460 magnetic field has also been carried out. An example is illustrated in Figure 5, showing a
461 snapshot of the coronal magnetic field with the formation of a sheared arcade structure in a
462 multipolar magnetic field structure (for the full animation, see Supplementary
463 Material, Streamer_shear_3d_view). The MFM approach allows to perform such
464 computations very rapidly (a couple of minutes on a laptop for axisymmetric cases) in
465 contrast to much more costly MHD-based methods. This allows time-dependent modeling
466 of the coronal magnetic field to be performed at a reasonable computational cost. Such
467 modeling is also radically different from PFSS as the latter does not include currents in the
468 model solution. Currently, methods of specifying the low-coronal boundary conditions
469 driving the evolution based on the methods of Lumme et al. (2017) are being evaluated.
470
471



472
473
474 **Figure 4:** Magneto-frictional relaxation simulation of a dipolar magnetic field to
475 include the stretching of the field due to solar wind outflows. At the left, the initial state

476
477
478
479
480

of the simulation is shown, while on the right, the relaxed state at the end of the simulation is shown.

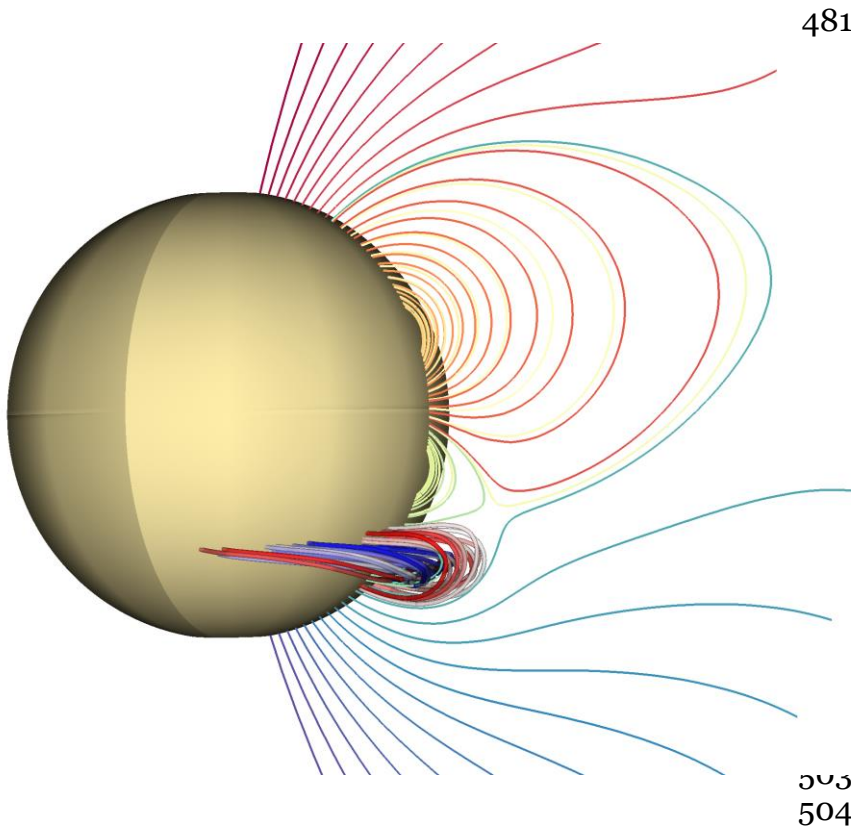


Figure 5: Formation of a sheared arcade structure in a multipolar magnetic field structure. The evolution of the Coronal field is efficiently computed using the MFM developed at University of Helsinki. This figure is a frame from a movie that is published as supplementary material to this paper.

505
506
507
508
509

510 3.1.2 Multi-VP model coupled to EUHFORIA

511 The physics-based model Multi-VP (Pinto and Rouillard, 2017) first makes a PFSS
512 extrapolation of a magnetogram and then solves the system of MHD equations describing
513 the heating and acceleration of a wind stream along a given magnetic flux-tube. Every such
514 flux tube is thus a 1D MHD wind solution. This is illustrated in Figure 6 using the WSO
515 magnetogram for CR2056 (2007 April-May) and showing a sample of magnetic field lines
516 obtained via PFSS extrapolation, which are used to initiate the model. Eventually, the total
517 of all these 1D solutions samples the whole solar atmosphere. Interpolation of the results on
518 a grid on a sphere at 0.1 AU, produces the MHD input file with density, pressure, magnetic
519 field and radial velocity distribution required for the heliospheric part of EUHFORIA.

520
521 In the framework of the ongoing validation of the solar wind modelling with EUHFORIA, we
522 implemented and tested the MULTI-VP model as an alternative coronal model, i.e. as an

523 alternative boundary condition for the heliospheric wind simulation in EUHFORIA. In other
524 words, we replaced the semi-empirical WSA+SCS based coronal model in EUHFORIA by
525 Multi-VP, and coupled it to the heliospheric wind model in EUHFORIA. In doing so, some
526 difficulties appear as there are a number of sub-Alfvénic speeds at 0.1 AU in the Multi-VP
527 output. These need to be transformed to (super-)Alfvénic because the boundary conditions
528 programmed in the heliospheric model assume that all boundary velocities are super-
529 Alfvénic. Therefore, the sub-Alfvénic pixels were replaced by interpolations using their first
530 super-Alfvénic neighbors while obeying the mass-flux conservation.

531
532 The first results and comparisons of EUHFORIA modelled output at Earth produced by
533 employing the WSA+SCS and MULTI-VP coronal models have been obtained. The Multi-VP
534 based boundary conditions turn out to better capture the fast solar wind streams. Figure 7
535 shows a 3D visualization of the structures produced by MULTI-VP+EUHFORIA-heliosphere
536 throughout the inner heliospheric domain for a solar minimum test case. The heliospheric
537 current sheet is indicated in grey while the colorful isosurfaces represent solar wind speeds
538 between 520 and 600 km/s. A demonstration of the spherical inner boundary surface can be
539 seen in the middle of the domain. It depicts the radial velocities at 0.1 AU. The Earth is shown
540 in light blue color and it can be seen that a fast solar wind stream hits the Earth, which is
541 also seen in WIND data. The standard EUHFORIA set-up with the WSA+SCS coronal model,
542 however, does not capture this fast wind stream at Earth, regardless of the magnetogram
543 used. Another HSS case during maximum, showed similar results. Samara et al. (2020)
544 showed that the choice of the coronal model as well as the choice of the magnetogram play
545 an important role on the quality of the solar wind forecast and conclude that a statistical
546 analysis is needed to confirm these findings.



Figure 6: The grey scale on the solar surface indicates the input WSO magnetogram in the MULTI-VP model for CR2056 (2007 April–May). A sample of magnetic field lines obtained via PFSS extrapolation used to initiate the model, are also depicted. The transparent yellow surface indicates the coronal hole boundaries (closed-field regions are excluded from the domain). For more details see Pinto & Rouillard, 2017.

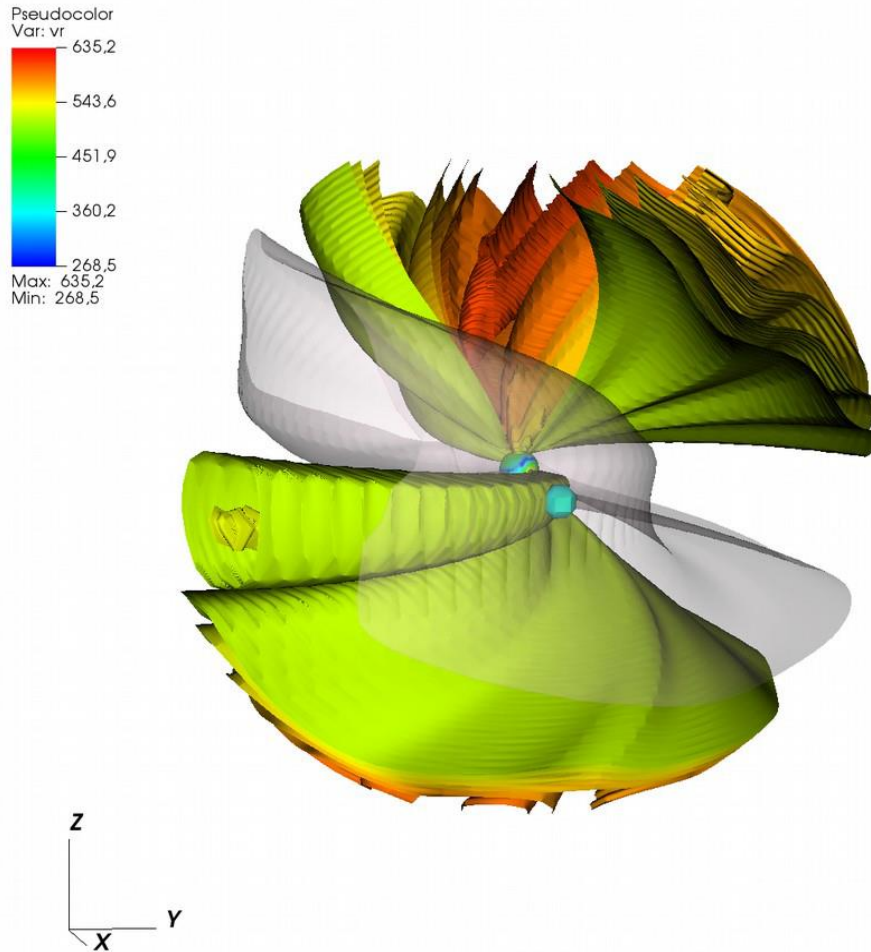


Figure 7: 3D visualization of the structures produced by MULTI-VP+ EUHFORIA-heliosphere throughout the inner heliospheric domain for the solar minimum test case. The heliospheric current sheet is indicated in grey while the colorful isosurfaces represent solar wind speeds between 520 and 600 km/s. A demonstration of the spherical inner boundary surface can be seen in the middle of the domain. It depicts the radial velocities at 0.1 AU. Earth is shown in light blue color.

599

600 3.1.3 Alternative CME flux-rope models

601 The current spheromak CME model in EUHFORIA (Verbeke et al. 2019; Scolini et al. 2019,
602 2020) significantly improves the predictions at L1 as compared to the ‘standard’ cone CME
603 model. Especially the magnetic field component predictions are much better and this, in
604 turn, yields better predictions of the geo-effectiveness of the CME impacts (Scolini et al.,
605 2020). However, the latter turns out to be true only in case of a ‘full hit’, when the ‘nose’ of
606 the CME hits the Earth. When the Earth is hit by a flank or ‘leg’ of the CME, the event cannot
607 be modelled very well with a spheromak model as this model does not have the typical flux-
608 rope shape of the CMEs. Therefore, we first implemented the Fri3D model (Isavnin, 2016)
609 as an alternative flux-rope CME model and this model is currently being tested (verification
610 of the modelling results and robustness of the implementation) before it will be committed
611 to the main EUHFORIA branch. A paper on the integration of the Fri3D flux-rope CME
612 model in EUHFORIA is in preparation.

613

614 An alternative toroidal flux-rope CME model has been implemented already and is also
615 currently being tested. The preliminary results show improved connectivity and magnetic

616 field profiles compared to the current spheromak-based model. As a matter of fact, this
 617 model also has the typical flux-rope shape of the CMEs and enables one to keep the CMEs
 618 connected to the Sun, as illustrated in Figure 8 which shows a snapshot of an EUHFORIA
 619 simulation with this novel CME model. In this particular case, the CME propagates at the
 620 interface of two slow and fast solar wind sections. The field line connected to the Earth is
 621 shown as the thick blue/green curve (with the small sphere indicating the position of the
 622 Earth). It can be seen that it exhibits a complex connectivity with the flux-rope magnetic
 623 field. During its evolution through the heliosphere, the flux-rope experiences significant
 624 asymmetric erosion, being more prominent at the western flank in this case, due to the
 625 interaction with the fast solar wind section.

626

627

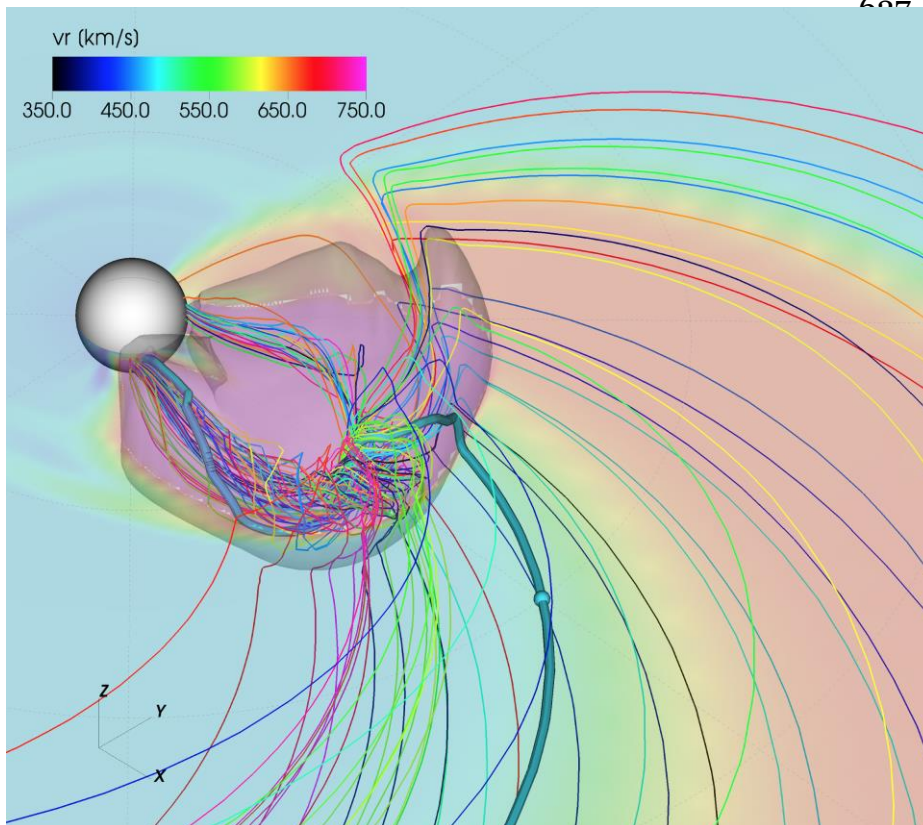


Figure 8: Snapshot of EUHFORIA simulation employing a toroidal flux rope currently being tested at University of Helsinki. The CME propagates at the interface of a slow and fast solar wind. The field line connected to Earth is shown as the thick blue/green curve and exhibits a complex connectivity with the flux rope magnetic field. The flux rope experiences significant asymmetric erosion, being more prominent at the western flank in this case.

652

653

654 3.1.4 Including solution adaptive mesh refinement techniques in EUHFORIA

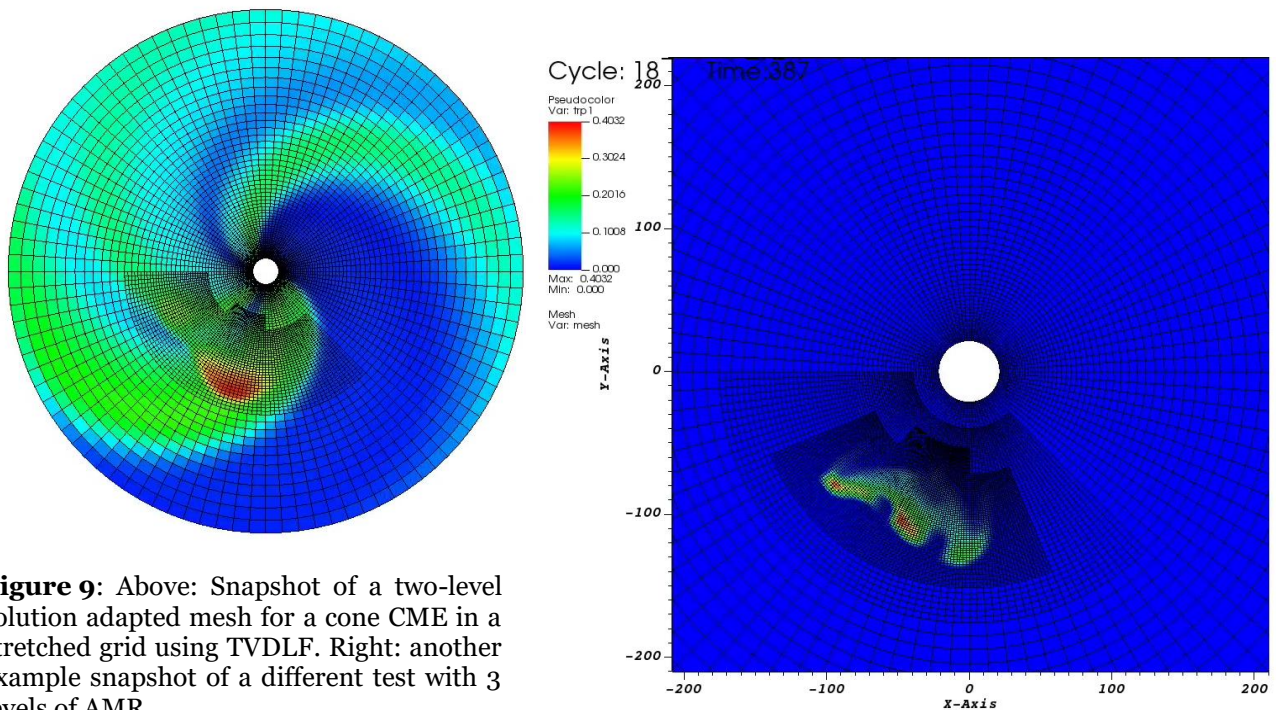
655 We also started working on a Finite Volume Method based implementation based on MPI-
 656 AMRVAC using a grid co-rotating with the Sun so that the obtained steady background wind
 657 is time-independent, unlike the current EUHFORIA set up using HEEQ coordinates, i.e. in
 658 which the Sun rotates in the grid and the Earth has a fixed longitude. A stretched grid has
 659 been implemented for the background wind and the effect of grid stretching combined with
 660 solution Adaptive Mesh Refinement (AMR) on the steady solar wind and evolving CMEs are
 661 being investigated. Grid stretching is especially useful in spherical geometries, because when
 662 the values of Δr , $\Delta \vartheta$, and $\Delta \varphi$ (using spherical coordinates (r, ϑ, φ)) are constant, the cell

663 widths become ever larger the further away from the grid center while the radial cell length
664 stays the same. This results in deformed grid cells which affects the numerical accuracy.
665 Applying grid stretching results in more regular 'cubic' grid cells resulting in a better
666 accuracy. Moreover, the simulation is faster on a stretched grid because there are much fewer
667 cells needed in the radial direction.
668

669 The first results have been verified (comparison with non-stretched grid results, timings,
670 convergence study, adjusted visualization, etc.) on realistic winds (based on magnetogram
671 extrapolations). Also, the cone CME model has already been implemented and is currently
672 being tested and convergence studies have been done.
673

674 Next, different AMR strategies are tested and timed, i.e. with AMR thresholds on different
675 quantities like density gradient, tracing function (tracing the CME plasma), velocity
676 divergence (which is negative at CIR and CME shocks, i.e. where particles can get accelerated
677 and AMR is thus useful), etc. and combinations of these, in order to fine-tune the AMR both
678 on the CIR shocks in the background solar wind and at the CME shock wave and magnetic
679 cloud (to study erosion and deformation, for instance). The results are very encouraging: the
680 stretching of the grid yields a better performance and speed-ups of 2.23 to 2.8 were obtained,
681 depending on the resolution. Combining AMR with grid stretching is much more efficient.
682 The performed tests yielded a speed-up of 13.97 using 2 grid levels (i.e. one refinement level)
683 and up to 99 when using 3 grid levels, limiting the higher resolution to the regions where
684 necessary. However, these speed-ups of course depend on the case under study and on the
685 refinement criteria applied. For instance, when there are multiple CIRs and/or multiple
686 CMEs, much more refinement area will be required and the speed-up is lower.

687
688



690 **Figure 9:** Above: Snapshot of a two-level
691 solution adapted mesh for a cone CME in a
692 stretched grid using TVDLF. Right: another
693 example snapshot of a different test with 3
694 levels of AMR.
695
696

697
698 Figure 9(left) shows a snapshot of such a CME evolution case using a two-level solution
699 adapted mesh for a cone CME in a stretched grid using a TVDLF solver. On the right-hand
700 side in this figure, another example is shown with a snapshot of a different test using 3 levels
701 of AMR in a more complex case where the CME is launched on an interaction of a slow and
702 a fast wind region. The colors correspond to the radial velocity component
703

704 The University of Helsinki team is also working on an alternative AMR strategy in the current
705 Constrained Transport scheme which guarantees the solenoidal condition ($\text{Div}(\mathbf{B})=0$) to be
706 satisfied up to machine accuracy. A preliminary example of the coronal model computed on
707 an AMR grid is shown in Figure 10, for a complicated case with many active regions.

708

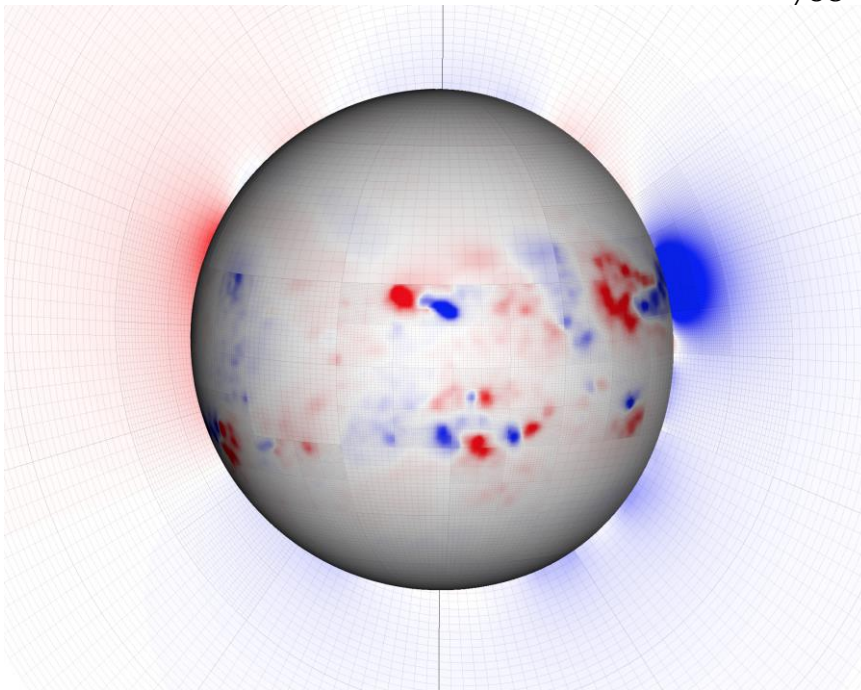


Figure 10: Preliminary example of the coronal model computed on an AMR grid using constrained transport - supported software being developed at University of Helsinki.

729
730

731
732

733 3.1.5 Evaluation of data-assimilation based on Kalman filtering for wind modelling

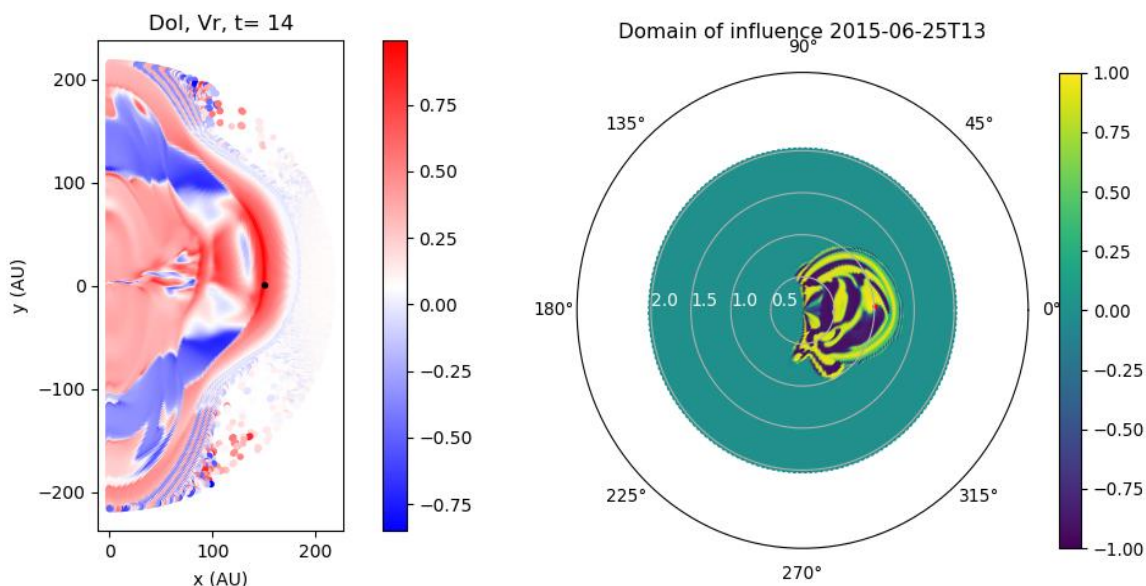
734 We applied a Representer and Domain of Influence analysis (Bennett, 1992; Echevin et al.,
735 2000; Evensen, 2009; Skandrani et al., 2014), which are powerful statistical tools that
736 enable to estimate the effectiveness of data assimilation techniques when applied to a
737 specific code or model, even before assimilating actual data. Representer analyses based on
738 the “Domain of Influence” (DoI) have already been tested on several different problems
739 related to space weather. The cases examined are the propagation of a CME against a
740 background solar wind using the codes EUHFORIA (in full 3D), and the propagation of a
741 CME against a background solar wind using the PLUTO code (in axisymmetric 2.5D
742 simulations), illustrated in Figure 11. The left panel of this figure shows the domain of
743 influence calculated from a PLUTO ensemble, using the radial velocity as a criterion, in the
744 meridional plane. The perturbed quantities are the radial velocity of the CME and its size.

745 This step was taken as a preliminary build-up phase to develop the tools in a reduced
746 dimensionality case. The right panel in Figure 11 shows the domain of influence calculated
747 from an EUHFORIA ensemble, but this time in the equatorial plane.
748

749 All tests use an ensemble of simulations, at least 50, where each member of the ensemble is
750 modified (compared to the reference run) using a perturbation selected from a Gaussian. We
751 then calculate the variance and the correlation of the ensemble using a physical quantity (e.g.
752 velocity) as a criterion.

753
754 In the EUHFORIA ensembles specifically, we first model the background solar wind using
755 real magnetograms. Then we inject a cone CME with different velocity and size in each
756 simulation. We tested additionally low- and high-resolution runs. We are currently
757 examining the effect of perturbations in the magnetograms.
758

759 The results of this study have been submitted for publication on a special issue of *Frontiers*
760 in *Astrophysics* dedicated to space weather modelling. The related paper is under review
761 (Millas et al., 2020).
762



763
764 **Figure 11:** Left: Domain of Influence calculated from a PLUTO ensemble, using the radial
765 velocity as a criterion, in the meridional plane. The perturbed quantities are the radial velocity
766 of the CME and its size. Right: Same, from an EUHFORIA ensemble, image on the meridional
767 plane.
768

769
770

771 3.1.6 Integration of SEP models – feasibility study

772

773 The SEP modelling approaches being developed by the team members have been evaluated
774 with respect to their potential to be applied in EUHFORIA 2.0. Regarding the transport
775 modelling of SEPs, there are three simulation models available, as mentioned before: the

776 PARADISE code of the KU Leuven, the DSPM code of the University of Turku, and the SaP
 777 code of the University of Barcelona. The SaP code requires the least CPU time and does seem
 778 to be the most appropriate to be integrated to obtain an operational model. However, it has
 779 been assessed that among these transport models, PARADISE has the broadest range of
 780 applicability in the various complex conditions that can take place in interplanetary space.
 781 Therefore, the next step has been to explore whether PARADISE, which uses forward Monte
 782 Carlo integration in time, is fast enough and can be applied directly or needs to be made
 783 more efficient.

784
 785 We have performed a scaling-test of the PARADISE model, using Skylake and the Broadwell
 786 processor architectures available on Tier-1 of the Flemish supercomputer (VSC). The results
 787 are depicted in Figure 12. For these simulations, protons were integrated forward in time for
 788 a physical time of 42 hours, using high-resolution runs of EUHFORIA as input. The solar
 789 wind was updated in PARADISE with a cadence of 5 minutes (physical time) on a grid with
 790 1024x80x360 grid points, leading to an I/O bound of $T_{I/O} \sim 47$ min and $T_{I/O} \sim 62$ min on the
 791 Skylake and Broadwell architectures, respectively. The figure below illustrates that
 792 PARADISE is an entirely parallel program, which is to be expected as there is no interaction
 793 between the simulated test-particles, and hence there is no communication necessary
 794 between the cores. Different options to reduce the I/O bound are being investigated,
 795 including the use of stretched grids in the radial direction, reducing the latitudinal extent of
 796 the grid, and increasing the snapshot cadence.
 797

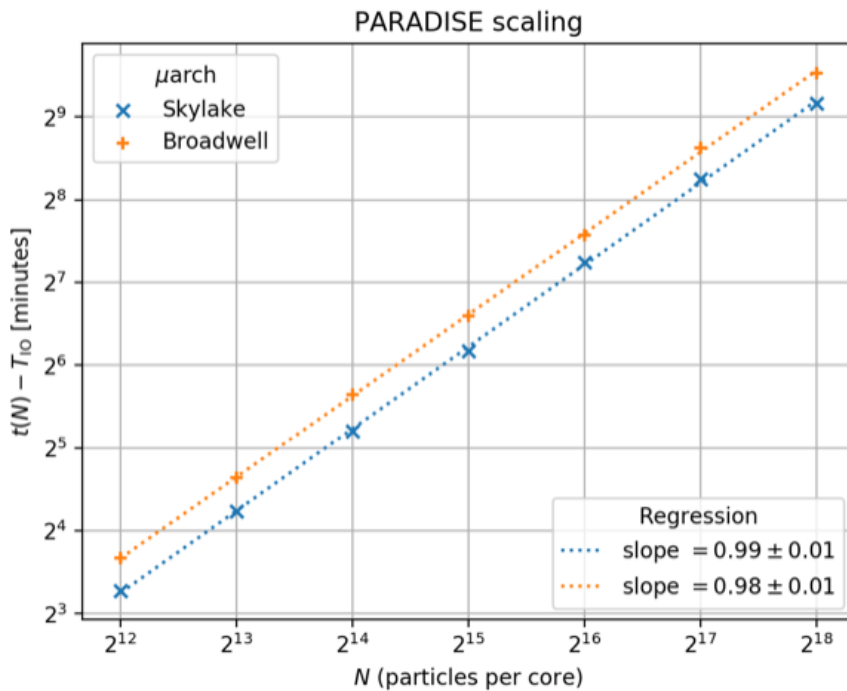


Figure 12: PARADISE scaling test results.

820

821 **4 BRIEF PRELIMINARY CONCLUSION**

822 The EU H2020-SPACE-2019 project EUHFORIA 2.0 started in December 2019 and involves
823 eleven research teams, supported by an ‘International Expert Advisory Panel’. The project
824 will develop an advanced space weather forecasting tool, combining an MHD solar corona
825 and wind model with one or more SEP models. The tool will be applied to study the
826 geoeffectiveness of the impacts of CMEs, CIRs and SEPs and will help to mitigate (part of)
827 the damage these cause. Extreme events will also be considered, though the emphasis will
828 be on improving the prediction of daily space weather and its effects. In particular, the effects
829 on forecasting Geomagnetically Induced Currents and radiation on geospace will be
830 addressed. The first results, obtained within the first six months of the project, have been
831 presented and the project is on schedule. The final innovative tool will be integrated into
832 both the Virtual Space Weather Modelling Centre (ESA) and the space weather forecasting
833 procedures at the ESA SSCC in Ukkel (Belgium), so that it will be available to the space
834 weather community and effectively used for improved predictions and forecasts of the
835 evolution of CME magnetic structures and their impact on Earth.
836
837

838 **Acknowledgements**

839 This project has received funding from the European Union’s Horizon 2020 research and
840 innovation programme under grant agreement No 870405. Additional support from the
841 projects C14/19/089 (C1 project Internal Funds KU Leuven), G.oDo7.19N (FWO-
842 Vlaanderen), C 90347 (ESA Prodex), Belpo BRAIN project BR/165/A2/CCSOM is greatly
843 acknowledged. For the computations at KU Leuven we used the infrastructure of the VSC –
844 Flemish Supercomputer Center, funded by the Hercules foundation and the Flemish
845 Government – department EWI.
846
847

848 **Bibliography**

- 849 Afanasiev, A., and Vainio, R. Monte Carlo Simulation Model of Energetic Proton Transport through Self-
850 generated Alfvén Waves. *Astrophys. J. Supp. Ser.* **207**:29, 2013. DOI: 10.1088/0067-0049/207/2/29
- 851 Afanasiev, A., Vainio, R., Kocharov, L. The Effect of Stochastic Re-acceleration on the Energy Spectrum of
852 Shock-accelerated Protons. *Astrophys. J.* **790**:36, 2014. DOI: 10.1088/0004-637X/790/1/36
- 853 Afanasiev, A., Battarbee, M., Vainio, R.. Self-consistent Monte Carlo simulations of proton acceleration in
854 coronal shocks: Effect of anisotropic pitch-angle scattering of particles. *A&A* **584**:81, 2015. DOI:
855 10.1051/0004-6361/201526750
- 856 Afanasiev, A., Aran, A., Vainio, R., Rouillard, A., Zucca, P., Lario, D., Barcewicz, S., Siipola, R., Pomoell, J.,
857 Sanahuja, B., Malandraki, O.E. Modelling of Shock-Accelerated Gamma-Ray Events. *Astrophysics and*
858 *Space Science Library* **444**:157, 2018a. DOI: 10.1007/978-3-319-60051-2_9
- 859 Afanasiev, A., Vainio, R., Rouillard, A. P., Battarbee, M., Aran, A., Zucca, P. Modelling of proton acceleration
860 in application to a ground level enhancement. *A&A* **614**:4, 2018b. DOI: 10.1051/0004-6361/201731343
- 861 Agostinelli, S., Allison, J., Amako, K.; Apostolakis, J., et al. GEANT4—a simulation toolkit. *Nuclear*
862 *Instruments and Methods in Physics Research A* **506**, 250-303, 2003. DOI: 10.1016/S0168-
863 9002(03)01368-8
- 864 Bacchini, F., Olshevsky, V., Poedts, S., & Lapenta, G. A new Particle-in-Cell method for modeling magnetized
865 fluids. *Computer Physics Comm.* **210**, 79-91, 2017. DOI: 10.1016/j.cpc.2016.10.001

- 866 Banjac, S., Herbst, K., Heber, B. The Atmospheric Radiation Interaction Simulator (AtRIS): Description and
867 Validation. *JGR: Space Physics*, **124**, 50–67, 2019. DOI: 10.1029/2018JA026042
- 868 Bennett, A. F. (1992). Inverse methods in physical oceanography (Cambridge university press). ISBN-13: 978-
869 0521055284
- 870 Bieber, J.W., Evenson, P., Dröge, W., Pyle, R., Ruffolo, D., Rujiwarodom, M., Tooprakai, P., Khumlumlert,
871 T. Spaceship Earth Observations of the Easter 2001 Solar Particle Event. *Astrophys. J. Lett.* **601**, L103–
872 L106, 2004. DOI: 10.1086/381801
- 873 Blelly, P. -L., A. Robineau, J. Lilensten, and D. Lummerzheim. 8-Moment Fluid Models of the Terrestrial High
874 Latitude Ionosphere Between 100 and 3000 KM. in *Solar Terrestrial Energy Program Ionospheric Model*
875 *Handbook*, edited by R.W. Schunk, pp. 53–72, Utah State Univ., Logan, 1996.
876 <https://www.bc.edu/content/dam/bc1/offices/ISR/SCOSTEP/Multimedia/other/ionospheric-models.pdf>
- 877 Blelly, P.-L. (2003), *SpaceGRID Study Final Report*. SGD-SYS-DAT-TN-100-1.2. Issue 1.2.
878 <https://www.yumpu.com/en/document/read/50039475/final-report-rss-esa>
- 879 Blelly, P. -L., Lathuillère, C., Emery, B., Lilensten, J., Fontanari, J., Alcaydé, D. An extended TRANSCAR
880 model including ionospheric convection: simulation of EISCAT observations using inputs from AMIE.
881 *Ann. Geophys.*, **23**, 419–431, 2005. DOI: 10.5194/angeo-23-419-2005
- 882 Caballero-Lopez, R.A. An estimation of the yield and response functions for the mini neutron monitor. *JGR*
883 *(Space Physics)* **121**, 7461–7469, 2016. DOI: 10.1002/2016JA022690
- 884 Caballero-Lopez, R.A., Moraal, H. Cosmic-ray yield and response functions in the atmosphere. *JGR: Space*
885 *Physics* **117**, A12103, 2012. DOI: 10.1029/2012JA017794
- 886 Desai, M., Giacalone, J. Large gradual solar energetic particle events. *Living Rev. Sol. Phys.* **13**:3, 2016. DOI:
887 10.1007/s41116-016-0002-5
- 888
- 889 Desorgher L, 2005, PLANETOCOSMICS Software User Manual Issue 0.1, 2006-06-14,
890 http://cosray.unibe.ch/~laurent/planetocosmics/doc/planetocosmics_sum.pdf
- 891 Echevin, V., De Mey, P., and
892 Evensen, G. (2000). Horizontal and vertical structure of the reparameter functions for sea surface
893 measurements in a coastal circulation model. *Journal of physical oceanography* **30**, 2627–2635. DOI:
894 10.1175/1520-0485(2000)030<2627:HAVSOT>2.0.CO;2
- 895 Evensen, G. (2009). Data assimilation: the ensemble Kalman filter (Springer Science & Business Media).
ISBN 978-3-642-03711-5
- 896 Farrugia, C.J., Jordanova, V.K., Thomsen, M.F., Lu, G., Cowley, S.W.H., Ogilvie, K.W. A two-ejecta event
897 associated with a two-step geomagnetic storm. *JGR: Space Physics* **111**, A11, 2006. DOI:
898 10.1029/2006JA011893
- 899 Fisk, L.A. & Lee, M.A. Shock acceleration of energetic particles in corotating interaction regions in the solar
900 wind. *Astrophys. J.* **237**, 620-626, 1980. DOI: 10.1086/157907
- 901 Heber, B., Galsdorf, D., Herbst, K., Gieseler, J., Labrenz, J., Schwerdt, C., Walter, M., Benadé, G., Fuchs, R.,
902 Krüger, H., Moraal, H. Mini neutron monitor measurements at the Neumayer III station and on the German
903 research vessel Polarstern. *Journal of Physics: Conference Series* **632**, 012057, 2015. DOI: 10.1088/1742-
904 6596/632/1/012057
- 905 Heck, D., Knapp, J., Capdevielle, J., Schatz, G., Thouw, T. CORSIKA: a Monte Carlo code to simulate
906 extensive air showers. Forschungszentrum Karlsruhe GmbH, Karlsruhe (Germany), V + 90 p., TIB
907 Hannover, D-30167 Hannover (1998). Bibcode: 1998cmcc.book.....H
- 908 Hurtaud, Y., C. Peymirat, and A. D. Richmond. Modeling seasonal and diurnal effects on ionospheric
909 conductances, region-2 currents, and plasma convection in the inner magnetosphere. *JGR* **112**, A09217,
910 2007. DOI: 10.1029/2007JA012257
- 911 Isavnin, A. FRiED: A Novel Three-dimensional Model of Coronal Mass Ejections.. *Astrophys. J.* **833**:267,
912 2016. DOI: 10.3847/1538-4357/833/2/267

- 913 Kelly, G. S., A. Viljanen, C. D. Beggan, and A. W. P. Thomson. Understanding GIC in the UK and French
 914 high-voltage transmission systems during severe magnetic storms. *Space Weather* **15**, 99-114 , 2017. DOI:
 915 10.1002/2016SW001469
- 916 Kilpua, E.K.J, Olsper, N., Grigorievskiy, A., Käpylä, M. J., Tanskanen, E. I., Miyahara, H., Kataoka, R., Pelt,
 917 J., Liu, Y. D. Statistical Study of Strong and Extreme Geomagnetic Disturbances and Solar Cycle
 918 Characteristics. *Astrophys. J.*, **806**:272, 2015. DOI:10.1088/0004-637X/806/2/272
- 919 Labrenz, J., Burmeister, S., Berger, T., Heber, B., Reitz, G. Matroshka DOSTEL measurements onboard the
 920 International Space Station (ISS). *J. Space Weather Space Clim.* **5**, A38, 2015. DOI: 10.1051/swsc/2015039
- 921 Lario, D. & Simnett, G.M. Solar Energetic Particle Variations. In *Solar Variability and Its Effects on Climate*,
 922 *Geophysical Monograph* **141**, 195-216, 2004. DOI: 10.1029/141GM14
- 923 Liu, J., Ye, Y., Shen, C., Wang, Y., Erdélyi, R. A New Tool for CME Arrival Time Prediction using
 924 Machine Learning Algorithms: CAT-PUMA. *Astrophys. J.*, **855**:109, 2018. DOI: 10.3847/1538-4357/aaae69
- 925 Liu, Y.D., Hu, H., Wand, R., Yand, Z., Zhu, B., Liu, Y.A., Luhman, J.G., Richardson, J.D. Plasma and
 926 magnetic field characteristics of solar coronal mass ejections in relation to geomagnetic storm intensity and
 927 variability. *Astrophys. J. Lett.*, **809**:L34, 2015. DOI:10.1088/2041-8205/809/2/L34
- 928 Lumme, E., Pomoell, J., Kilpua, E.K.J. Optimization of Photospheric Electric Field Estimates for Accurate
 929 Retrieval of Total Magnetic Energy Injection. *Solar Phys.*, **292**, A191, 2017. DOI 10.1007/s11207-017-
 930 1214-0
- 931 Magdalenic, J., Marqué, C., Krupar, V, Mierla, M., Zhukov, A.N., Rodriguez, L., Maksimović, M., Cecconi,
 932 B. Tracking the CME-driven Shock Wave on 2012 March 5 and Radio Triangulation of Associated Radio
 933 Emission. *Astrophys. J.* **791**, 115, 2014. DOI: 10.1088/0004-637X/791/2/115
- 934 Marchaudon, A., and P.-L. Blelly. A new interhemispheric 16-moment model of the plasmasphere-ionosphere
 935 system: IPIM. *JGR: Space Physics* **120**, 5728-5745, 2015. DOI: 10.1002/2015JA021193
- 936 Millas, D., Innocenti, M.E., Laperre, B., Raeder, J., Poedts, S., Lapenta, G. The effectiveness of Data
 937 Assimilation in Space Weather forecasting: heliospheric and magnetospheric applications via MHD
 938 simulations. *Frontiers in Astrophysics*, submitted (2020).
- 939 Mishev, A., and Usoskin, I. Numerical model for computation of effective and ambient dose equivalent at
 940 flight altitudes. Application for dose assessment during GLEs. *J. Space Weather Space Clim.* **5**, A10, 2015.
 941 DOI: 10.1051/swsc/2015011
- 942 Möller, T., Burda, O., Burmeister, S., Heber, B., Langner, F., Wissmann, F. In-field calibration of the
 943 Navigation Dosimetry System (NAVIDOS) during solar minimum conditions. *Astrophysics and Space
 944 Sciences Transactions* **8**, 45–49, 2012. DOI: 10.5194/astra-8-45-2012
- 945 Odstroil D. Modeling 3-D solar wind structure. *Advances in Space Research* **32** (4), 497-506, 2003. DOI:
 946 10.1016/S0273-1177(03)00332-6
- 947 O’Neill, P.M. Badhwar–O’Neill 2010 Galactic Cosmic Ray Flux Model—Revised. *IEEE Transactions on
 948 Nuclear Science* **57** (6), 3148–3153, 2010. DOI: 10.1109/TNS.2010.2083688
- 949 Owens, M.J., and Forsyth, R.J. The Heliospheric Magnetic Field. *Living Rev. Sol. Phys.* **10**: 5, 2013. DOI:
 950 10.12942/lrsp-2013-5
- 951 Pinto, R. F., Rouillard, A. P. A Multiple Flux-tube Solar Wind Model. *Astrophys. J.* **838**: 89, 2017. DOI:
 952 10.3847/1538-4357/aa6398
- 953 Poedts S. Forecasting space weather with EUHFORIA in the Virtual Space Weather Modeling Centre,
 954 *Plasma Physics and Controlled Fusion*, **61**, 014011, 2018. DOI: 10.1088/1361-6587/aae048
- 955 Poedts S., A. Kochanov, A. Lani, C. Scolini, C. Verbeke, S. Hosteaux, E. Chané, H. Deconinck, N.
 956 Mihalache, F. Diet, D. Heynderickx, J. De Keyser, E. De Donder, N.B. Crosby, M. Echim, L. Rodriguez,
 957 R. Vansintjan, F. Verstringe, B. Mampaey, R. Horne, S. Glauert, P. Jiggins, R. Keil, A. Glover, G.
 958 Deprez, J.-P. Luntama. The Virtual Space Weather Modelling Centre. *J. Space Weather Space Clim.*, **10**,
 959 A14, 2020. DOI: 10.1051/swsc/2020012

- 960 Pomoell J., Aran A., Jacobs C., Rodríguez-Gasén R., Poedts S., Sanahuja B. Modelling large solar proton
961 events with the shock-and-particle model. Extraction of the characteristics of the MHD shock front at the
962 cobpoint. *J. Space Weather Space Clim.* **5**, A12, 2015. DOI: 10.1051/swsc/2015015
- 963 Pomoell, J., Lumme, E., Kilpua, E. Time-dependent Data-driven Modeling of Active Region Evolution
964 Using Energy-optimized Photospheric Electric Fields. *Solar Phys.*, **294**:41, 2019. DOI: 10.1007/s11207-
965 019-1430-x
- 966 Pomoell J. and Poedts S. EUHFORIA: European heliospheric forecasting information asset. *J. Space*
967 *Weather Space Clim.*, **8**, A35, 2018. DOI: 10.1051/swsc/2018020
- 968 Pomoell J. and Vainio R. Influence of Solar Wind Heating Formulations on the Properties of Shocks in the
969 Corona. *Astrophys. J.* **745**:151, 2012. DOI:10.1088/0004-637X/745/2/151
- 970 Price, D.J., Pomoell, J., Lumme, E., Kilpua, E.K.J. Time-dependent data-driven coronal simulations of AR
971 12673 from emergence to eruption. *Astron. Astrophys.*, **628**, A114, 2019. DOI: 10.1051/0004-
972 6361/201935535
- 973 Raeder, J., Cramer, W.D., Germaschewski, K., Jensen, J. Using OpenGGCM to Compute and Separate
974 Magnetosphere Magnetic Perturbations Measured on Board Low Earth Orbiting Satellites. *Space Science*
975 *Rev.* **206**:601, 2017. DOI: 10.1007/s11214-016-0304-x
- 976 Riley, P. On the probability of occurrence of extreme space weather events. *Space Weather* **10**, S02012,
977 2012. DOI: 10.1029/2011SW000734
- 978 Samara, E., Pinto, F.P., Magdalenic, J., Jercic, V., Scolini, C., Wijzen, N., Jebaraj, I.C., Rodriguez, L.,
979 Poedts, S.. Implementing the MULTI-VP coronal model in EUHFORIA: results and comparisons with the
980 WSA coronal model. Submitted to *Astron. Astrophys.*, 2020.
- 981 Schrijver, K., Kauristie, K., Aylward, A., Denardini, C. M., et al. Understanding space weather to shield
982 society: A global road map for 2015–2025 commissioned by COSPAR and ILWS. *Advances in Space*
983 *Research* **55**, Issue 12, 2745-2807, 2015. DOI: 10.1016/j.asr.2015.03.023
- 984 Scolini C., Rodriguez, L., Mierla, M., Pomoell, J., Poedts, S. Observation-based modelling of magnetised
985 coronal mass ejections with EUHFORIA, *Astron. Astrophys.*, **626**, A122, 2019. DOI: 10.1051/0004-
986 6361/201935053
- 987 Scolini C., E. Chané, M. Temmer, E. Kilpua, K. Dissauer, A.M. Veronig, E. Palmerio, J. Pomoell, M.
988 Dumbović, J. Guo, L. Rodriguez, S. Poedts. CME—CME Interactions as Sources of CME
989 Geoeffectiveness: The Formation of the Complex Ejecta and Intense Geomagnetic Storm in 2017 Early
990 September. *Astrophys. J. Supl. series*, **247** (1), Art. 21, 2020. DOI: 10.3847/1538-4365/ab6216
- 991 Shiota, D. and Kataoka, R. Magnetohydrodynamic simulation of interplanetary propagation of multiple
992 coronal mass ejections with internal magnetic flux rope (SUSANOO-CME). *Space Weather* **14**, Issue 2,
993 56-75, 2015. DOI:10.1002/2015SW001308
- 994 Skandrani, C., Innocenti, M. E., Bettarini, L., Crespon, F., Lamouroux, J., and Lapenta, G. (2014). Flip-mhd-
995 based model sensitivity analysis. *Nonlinear processes in geophysics* **21**, 539–553. DOI: 10.5194/npg-
996 21-539-2014
- 997 Thomson, A.W.P., McKay, A.J., Clarke, E., and Reay, S. Surface electric fields and geomagnetically induced
998 currents in the Scottish Power grid during the 30 October 2003 geomagnetic storm. *Space Weather* **3**,
999 S11002, 2005. DOI: 10.1029/2005SW000156
- 1000 Tóth, G., Sokolov, I.V., Gombosi, T.I., et al. Space Weather Modeling Framework: A new tool for the space
1001 science community. *JGR Space Physics* **110**, A12226, 2005. DOI: 10.1029/2005JA011126
- 1002 Vainio R., Laitinen T. Monte Carlo Simulations of Coronal Diffusive Shock Acceleration in Self-generated
1003 Turbulence. *Astrophys. J.* **658**:622, 2007. DOI: 10.1086/510284
- 1004 Vainio R., Pönni A., Battarbee M., Koskinen E.J., Afanasiev A., Laitinen T. A semi-analytical foreshock model
1005 for energetic storm particle events inside 1 AU. *J. Space Weather Space Clim.*, **4**, A08, 2014. DOI:
1006 10.1051/swsc/2014005

- 1007 Van der Holst, B, Sokolov, I.V., Meng, X., Jin, M., Manchester, W.B. IV, Tóth, G., Gombosi, T.I. Alfvén
1008 Wave Solar Model (AWSoM): Coronal Heating. *Astrophys. J.* **782**, 81, 2014. DOI: 10.1088/0004-
1009 637X/782/2/81
- 1010 Verbeke C., Pomoell J., and Poedts S. The Evolution of Coronal Mass Ejections in the Inner Heliosphere:
1011 Implementing the Spheromak Model with EUHFORIA. *Astron. Astrophys.*, **627**, A111, 2019. DOI:
1012 10.1051/0004-6361/201834702
- 1013 Vršnak, B., Magdaleníć, J., and Zlobec, P. Band-splitting of coronal and interplanetary type II bursts. III.
1014 Physical conditions in the upper corona and interplanetary space. *Astron. Astrophys.* **413**, 753, 2004. DOI:
1015 10.1051/0004-6361:20034060
- 1016 Webb, D.F. and Howard, T.A. Coronal Mass Ejections: Observations. *Living Rev. Solar Phys.*, **9**, A3, 2012.
1017 DOI: 10.12942/lrsp-2012-3
- 1018 Wijzen, N. PARADISE: a model for energetic particle transport in the solar wind. Dissertation presented in
1019 partial fulfilment of the requirements for the degree of Doctor of Science (PhD): Mathematics (KU
1020 Leuven) and the degree of Doctor of Physics (Universitat de Barcelona). April 2020.
- 1021 Wijzen N., Aran A., Poedts S., Pomoell J. Modelling three-dimensional transport of solar energetic protons in
1022 a corotating interaction region generated with EUHFORIA. *Astron. Astrophys.*, **622**, A28, 2019a. DOI:
1023 10.1051/0004-6361/201833958
- 1024 Wijzen N., Aran A., Pomoell J., Poedts S. The Interplanetary Spread of Solar Energetic Protons Near a High-
1025 Speed Solar Wind Stream. *Astron. Astrophys.*, **634**, A47, 2019b. DOI: 10.1051/0004-6361/201935139
- 1026 Wintoft, P., Wik, M., Viljanen, A. Solar wind driven empirical forecast models of the time derivative of the
1027 ground magnetic field. *J. Space Weather Space Clim.*, **5**, A7, 2015. DOI: 10.1051/swsc/2015008